COBEM2003 - 0567 Copyright © 2003 by ABCM

NUMERICAL INVESTIGATION ON GAS-DISPLACEMENT OF VISCOELASTIC LIQUIDS IN CAPILLARY TUBES

Edson J. Soares
Departament of Mechanical Engineering
Universidade Federal do Espírito Santo (UFES)
Av. Fernado Ferrari s/ n, Goiabeiras
29060-900, Vitória, ES, Brazil
ejsoares2001@yahoo.com.br

Paulo Roberto de Souza Mendes
Department of Mechanical Engineering
Pontifícia Universidade Católica do Rio de Janeiro (PUC-Rio)
Rua Marquês de São Vicente 225, Gávea
22453-900, Rio de Janeiro, RJ, Brazil
pmendes@mec.puc-rio.br

Márcio da S. Carvalho
Department of Mechanical Engineering
Pontifícia Universidade Católica do Rio de Janeiro (PUC-Rio)
Rua Marquês de São Vicente 225, Gávea
22453-900, Rio de Janeiro, RJ, Brazil
msc@mec.puc-rio.br

Abstract. The displacement of a fluid in a capillary tube by gas injection occurs in many practical applications like enhanced oil recovery, coating of catalytic converters and gas-assisted injection molding. Other quite important application is the analysis of mucus displacement in pulmonary airways. The gas-displacement has been extensively studied both by theory and experiments in the case of Newtonian fluids. However, the complete understanding of rheological effects properties of the displaced fluid in this type of flow is still under investigation. The flow of viscoelastic liquids has been analyzed experimentally by measuring the fractional coverage of the tube wall and by Particle Tracking Velocimetry. The main conclusion was that the flow near the interface presents strong extensional deformation and the viscoelastic behavior of the liquid leads to a larger deposited liquid layer on the wall. Flow simulations with non Newtonian liquids for this situation are rare. The presence of free surface and non linearities of the constitutive model make the problem extremely complex. In this work, the complete two dimensional solution of free surface flow is obtained using the Galerkin finite element method. The rheological character of the liquid is modelled by two different constitutive equations: a simple Generalized Newtonian Liquid model, to analyze the effect of shear sensitive liquids; and the algebraic constitutive relation proposed by Thompson et al. (1999) that is capable of describing variable shear and extensional viscosity, first normal stress coefficient and second normal stress coefficient. This constitutive equation is used to analyze the effect of the viscoelastic properties of the liquid on the flow field.

Keywords. *gas displacement 1, viscoelastic liquids 2, finite element method 3, free surface flows 4*

1. Introduction

The gas displacement of a fluid in a capillary tube occurs in many practical applications like enhanced oil recovery, coating of catalytic converters and gas-assisted injection molding. Other quite important application is the study of mucus displacement in pulmonary airways by a rigid capillary approximation. As the gas pushes the liquid through the tube, a thin liquid layer is left attached to the wall. The thickness of this liquid film is an important parameter in many of the applications mentioned before: in the case of oil recovery, the amount of liquid left on the wall determines the efficiency of the recovery process; in the case of gas-assisted injection molding, the thickness of the layer will determine the strength of the hollow part produced; and in the case of analysis of mucus displacement in pulmonary airways, the fraction of material left behind will indicate the grade of obstruction on the airways.

The flow of a gas penetrating a Newtonian liquid has been extensively studied both by theory and experiments. The goal was to understand the flow near the gas-liquid interface in order to determine the amount of liquid left on the tube wall as a function of the operating parameters and liquid properties.

However, in many of the practical applications, as those referred before, the liquid being displaced is a polymer melt, a solution or a dispersion that shows non Newtonian behavior. The complete understanding of the effects of the rheological properties of the displaced liquid in this type of flow is still under investigation.

The thickness of the thin liquid layer attached to the wall is usually characterized in terms of the fractional deposited mass m, defined in Eq. (1). R_0 is the tube radius and R_b is the radius of the cylindrical portion of the gas bubble, as illustrated in Fig. (1-a). The fractional mass can also be evaluated as a function of the bubble velocity V_b and the mean velocity $\overline{u}$ of the liquid ahead of it.

$$m = \frac{mass\ left\ on\ the\ wall}{total\ mass} = 1 - \frac{displaced\ mass}{total\ mass} = 1 - \left(\frac{R_b}{R_o}\right)^2 = \frac{V_b - \bar{u}}{V_b} \tag{1}$$

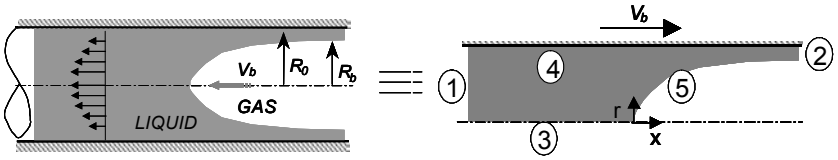

Figure 1. a- Sketch of gas displacement of a liquid in a capillary tube. b- Flow domain for gas displacement of liquids in a tube in a reference frame located on tip of the interface. The numbers 1 to 5 represent the sections where the boundary conditions are posed.

The first experimental analysis of gas-assisted displacement was done by Fairbrother and Stubs (1935). They found an expression for m valid at small capillary numbers $Ca \equiv \mu V_b / \sigma$ and Newtonian liquid:

$$m = Ca^{1/2} \tag{2}$$

Taylor (1960) studied the same problem for a much larger range of capillary number. He found that the mass deposited on the tube wall asymptotically approaches 0.55 as Ca approaches 2. Taylor also suggested three possible streamline patterns of the liquid flow near the interface. At high capillary number, the flow would pass completely and no recirculation would appear near the free surface. The other two patterns would occur at intermediate to low capillary numbers, and they would be characterized by the position of the recirculation near the free surface.

Cox (1962), continuing Taylor's study for a Newtonian viscous fluid, found experimentally that the amount of mass deposited on the tube wall asymptotically reaches 0.60 as the capillary number approaches 10. Cox also predicted the shape of the interface using perturbation analysis. He concluded in his experiments that the flow is sensitive to the presence of the interface only in a region about one and a half the tube diameter ahead the nose of the bubble. Furthermore, he concluded that the bubble reaches its final shape after it flows the same distance (one and a half the tube diameter). In a second work, Cox (1964) investigated experimentally the streamline patterns suggested by Taylor and found a good agreement in the cases of high and low capillary number.

Bretherton (1960) investigated theoretically and experimentally the motion of long gas bubbles in tubes filled with Newtonian viscous liquid. He found a simple theoretical relationship for the mass deposited on the tube wall m, valid at low capillary number, that agrees well with Fairbrother and Stubs (1935) experimental measurements:

$$m = 2.68 Ca^{2/3} \tag{3}$$

The penetration of long gas bubble in a viscoelastic liquid was studied experimentally by Huzyak and Koelling (1997). They were interested in identifying the influence of viscoelastic behavior on the fraction of the mass deposited on the tube wall. The experiments were performed with highly elastic liquid with constant shear viscosity. The results were presented in terms of capillary number Ca and Deborah number De. They found that the fractional mass deposited on the wall begins to increase, relatively to Newtonian fluid, for $De \geq 1$ and continues increasing over the entire range of De analyzed. Following the work of Huzyak and Koelling, Gauri and Koelling (1999) analyzed the kinematics of the flow near the free surface using Particle Tracking Velocimetry (PTV).

The effect of shear thinning behavior of the displaced liquid in this type of flow was studied by Poslinski and Coyle (1994). They used the Finite Element Method to solve the two dimensional model of the flow. Kamisli and Rayan (1999) performed experiments and showed that the thickness of the deposited layer falls with the power-law index. They presented a singular perturbation analysis to model this situation, but their predictions followed an opposite trend of the experimental results.

Theoretical analysis of the effect of different rheological properties other than the shear dependent viscosity is rare. The presence of the free surface and the non-linearities of the constitutive models make the problem extremely complex.

One possible approach to model gas penetration through a viscoelastic liquid is to use differential constitutive equations, such as Giesekus model. However, the solution of the momentum equation coupled with this type of constitutive equations is a major numerical challenge and solutions can not be obtained at the range of dimensionless parameters that occurs in practical applications. An alternative way is to use algebraic models that relate stress to the rate-of-strain and relative-rate-of-rotation. These models are perhaps the simplest and computationally most economical attempt at capturing the different behavior of polymer molecules in extension-dominated and shear-dominated flow zones. Recent advances developed by Thompson at al (1999) in this class of models have produced a constitutive

relation that describes shear thinning and normal stress differences in simple shear flow and extensional thickening in extensional flows. This tactic is pursued here.

In this work, the complete two dimensional solution of the free surface flow is obtained using the Galerkin finite element method. The rheological character of the liquid is modelled by two different constitutive equations: a simple Generalized Newtonian Liquid model, to analyze the effect of shear sensitive liquids; and the algebraic constitutive relation proposed by Thompson et al (1999). This equation is used to analyze the effect of the viscoelastic properties of the liquid on the flow field. The theoretical predictions are compared with some of the experimental data for non Newtonian liquids available in the literature.

2. Stead gas penetration model

When a gas is injected at a constant rate in a capillary tube displacing a liquid, a thin layer of liquid is left on the wall of the tube. The thickness of this layer is important in many of the processes described in the previous section and is a strong function of the operating conditions and liquid properties.The flow near the gas-liquid interface is analyzed using a moving reference frame placed at the tip of the bubble, as shown in Fig.(1-b). In this figure, the interface is moving from right to left. Relative to the reference frame, the capillary tube wall moves with the interface velocity V_b and the interface is stationary.

2.2. Conservation Equations and Boundary Conditions

The flow near the interface is two-dimensional and axisymmetric. The velocity and pressure fields, and the configuration of the gas-liquid interface are governed by the momentum, Eq. (5) and continuity, Eq. (4), together with the appropriate boundary conditions.

$$\nabla \cdot \mathbf{u} = 0 \tag{4}$$

$$\rho \mathbf{u} \cdot \nabla \mathbf{u} = \nabla \cdot \mathbf{T} \tag{5}$$

Here **u** is the velocity field and **T** is the stress tensor.
Far enough upstream of the interface, boundary (1), the flow is taken to be fully developed and the pressure constant:

$$\mathbf{n} \cdot \nabla \mathbf{u} = \mathbf{0} \quad \text{and} \quad p = P_{in} \tag{6}$$

Far enough downstream, boundary (2), the liquid traction vanishes:

$$\mathbf{n} \cdot \mathbf{T} = \mathbf{0} \tag{7}$$

Along the symmetry axis (3), the shear stress and the radial velocity vanish:

$$\mathbf{t} \cdot [\mathbf{n} \cdot \mathbf{T}] = 0 \quad \text{and} \quad \mathbf{n} \cdot \mathbf{u} = \mathbf{0} \tag{8}$$

The no-slip and no-penetration conditions are applied along the tube wall (4):

$$\mathbf{u} = \mathrm{V_b} \mathbf{e}_x \tag{9}$$

Over the gas-liquid interface (5), the traction in the liquid balances the capillary pressure and there is no mass flow across the interface

$$\mathbf{n} \cdot \mathbf{T} = \left(\frac{\sigma}{R_m} - P_o \right) \mathbf{n} \quad \text{and} \quad \mathbf{n} \cdot \mathbf{u} = 0 \tag{10}$$

Here σ is the liquid surface tension, **n** is the unit normal vector to the free surface and $1/R_m$ is the local mean curvature of the interface.

2.3. Constitutive Models

In order to close the set of differential equations, the stress tensor has to be related with the kinematics of the flow. Here, two different non Newtonian models are used. The first is a simple Generalized Newtonian Model with a Power-

Law viscosity function. The second is the algebraic model proposed by Thompson et al. (1999) that takes into account the different behavior of polymer molecules in extension-dominated and shear-dominated flow zones.

2.3.1. Generalized Newtonian Model: Power-law viscosity

In this simple model, the stress tensor is given by

$$\mathbf{T} = -p\mathbf{I} + \eta(2\mathbf{D})2\mathbf{D}, \tag{11}$$

where $2\mathbf{D} \equiv \nabla\mathbf{v} + \nabla\mathbf{v}^T$ is the rate of strain tensor. η is the liquid viscosity, which is a function of the deformation of the flow. In the particular case of a Power-Law viscosity function, it is given by

$$\eta = K\dot{\gamma}^{n-1} \tag{12}$$

n is the power-law index and $\dot{\gamma}$ is the local deformation rate.

2.3.2. Algebraic Viscoelastic Model

The algebraic model used here was proposed by Thompson et al. (1999). The stress tensor is a function of both the rate-of-strain tensor $2\mathbf{D}$ and the relative-rate-of-rotation tensor $\overline{\mathbf{W}}$:

$$\mathbf{T} = \alpha_0\mathbf{I} + \alpha_1\mathbf{D} + \alpha_3\mathbf{D}^2 + \alpha_4\left(\mathbf{D}\cdot\overline{\mathbf{W}} - \overline{\mathbf{W}}\cdot\mathbf{D}\right) \tag{13}$$

The relative-rate-of-rotation tensor is defined as $\overline{\mathbf{W}} = \mathbf{W} - \mathbf{\Omega}$, where $\mathbf{W} = \nabla\mathbf{v} - \nabla\mathbf{v}^{\mathbf{T}}$ is the vorticity tensor, and the tensor $\mathbf{\Omega}$ is the rate of rotation of the eigenvectors of the rate of strain. Based on the rate-of-strain and relative-rate-of-rotation tensors, Astarita (1979) defined the flow classification index R to measure the degree to which the fluid particle avoids stretching. It is defined as

$$R \equiv -\frac{tr(\overline{\mathbf{W}})}{tr(\mathbf{D})} \tag{14}$$

The index takes the value of 0 in pure extension and 1 in shear flows. Moreover, as the motion approaches a rigid body motion, i.e. as $\mathbf{D} \to 0$, it approaches infinity.

The coefficients $\alpha_i{}'s$ depend on the material functions of the liquid:

$$\alpha_0 = -\,\mathrm{p} - \frac{1}{3}\alpha_3\mathrm{tr}\mathbf{D}^2;\ \alpha_1 = 2\eta_s^R\eta_u^{1-R}\ ;\ \alpha_3 = f\left(\Psi_1, \Psi_2, \eta_u, R\right) \text{ and } \alpha_4 = R\psi_1 \tag{15}$$

The additional definitions needed before using Eq. (13) are the forms of the functions $\eta_s, \eta_u, \psi_1,$ and ψ_2. One of the advantages of using such class of models is that the measurements of these material functions in shear and extensional flows can be independently fitted.

According to Thompson et al. (2002), the extensional viscosity can be divided in two parts, one dissipative and other elastic, defined as

$$\eta_u = \beta\eta_u + (1-\beta)\eta_u \tag{16}$$

$\beta\eta_u$ represents the dissipative portion and $(1-\beta)\eta_u$ represents the elastic portion. For the limit case, $\beta = 1$, the function α_3 must vanish in pure extensional flow. Hence, it can be calculated as

$$\alpha_3 = \left[2\psi_1 + 4\psi_2\right]R \tag{17}$$

For the other limit case, $\beta = 0$, α_1 reduces to the case of Generalized Newtonian Model, and thus, independent of R.

$$\alpha_1 = 2\eta_s \tag{18}$$

Furthermore, the function α_3 makes the connection between the extensional viscosity, η_u, and the normal stress difference coefficients ψ_1 and ψ_2.

$$\alpha_3 = \left[2\psi_1 + 4\psi_2\right] R + \left[\frac{4(T_R - 1)}{\eta_s \dot{\varepsilon}}\right](1 - R) \tag{19}$$

Here, $T_R = \eta_u / \eta_s$ and $\dot{\varepsilon}$ is the extension rate.

In the predictions presented in this work, the shear viscosity and the normal stress difference coefficients were constants and the extensional viscosity was a known function of the deformation rate, i.e.

$$\eta_u = \eta_0 \left\{1 + (\lambda_u \dot{\gamma})^2\right\}^{\frac{n_u - 1}{2}} \tag{20}$$

Here, η_0 is the viscosity in zero shear rate, n_u a power index and λ_u is a characteristic time.

3. Solution Method

Because of the free surfaces, the flow domain for each parameter is unknown a priori. In order to solve this free boundary problem by means of standard techniques for boundary value problems, the set of differential equations and boundary conditions posed in the unknown domain has to be transformed to an equivalent set defined in a known reference domain. This transformation is made by a mapping $\mathbf{x} = \mathbf{x}(\boldsymbol{\xi})$ that connects the two domains, as shown in Fig. (2). The unknown physical domain is parameterized by the position vector $\mathbf{x}$, and the reference domain by $\boldsymbol{\zeta}$. A functional of weighted smoothness can be used successfully to construct the sorts of maps involved here. The inverse of the mapping that minimizes the functional is governed by a pair of elliptic differential equations identical with those encountered in diffusional transport with variable diffusion coefficients. The coordinates ξ and η of the reference domain satisfy

$$\nabla \cdot \left(D_\xi \nabla \xi\right) = 0 \quad \text{and} \quad \nabla \cdot \left(D_\eta \nabla \eta\right) = 0 \tag{21}$$

D_ξ and D_η are diffusion-like coefficients used to control element spacing. Equations (3.1-a) and (3.1-b) describe the inverse mapping $\boldsymbol{\xi} = \boldsymbol{\xi}(\mathbf{x})$. To evaluate $\mathbf{x} = \mathbf{x}(\boldsymbol{\xi})$, the diffusion equations that describe the mapping also have to be transformed to the reference configuration. The gradient of mapping $\mathbf{x} = \mathbf{x}(\boldsymbol{\xi})$ in a two dimensional domain is defined as $\nabla_\xi \mathbf{x} = \mathbf{J}$. $\|J\| = \det \mathbf{J}$ is the Jacobian of the transformation. Boundary conditions are needed in order to solve the second-order partial differential equations, Eq. (3.1-a) and Eq.(3.1-b).

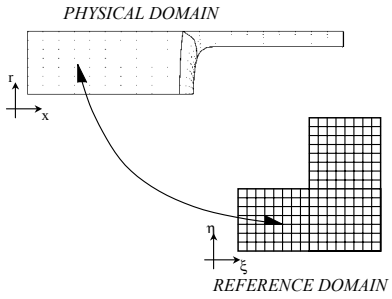

Figure 2. Mapping between physical and reference domain.

Along solid walls and synthetic inlet and outlet planes, the boundary is located by imposing a relation between the coordinates x and r from the equation that describes the shape of the boundary and stretching functions are used to distribute the points along the boundaries. The free boundaries (gas-liquid interfaces) are located by imposing the kinematic condition, Eq. (2.7-b). The discrete version of the mapping equations is generally referred to as mesh generation equations.

The differential equations the that govern the problem and the mapping (mesh generation) equations were solved all together by the Galerkin / finite element method. The velocity, pressure and node position are represented in terms of the appropriate basis functions.

$$u = \sum_{j=1}^{n} U_j \phi_j \; ; \; v = \sum_{j=1}^{n} V_j \phi_j \; ; \; p = \sum_{j=1}^{m} P_j \chi_j \; ; \; x = \sum_{j=1}^{n} X_j \phi_j \; ; \; r = \sum_{j=1}^{n} R_j \phi_j \tag{22}$$

Biquadratic bases function (ϕ_j) were used to represent the velocity and nodal coordinates and linear discontinue functions (χ_j) to expand the pressure field. Because the stress tensor depends on the second derivative of the velocity field (through the definition of the index R), an additional variable **L** is introduced to represent the velocity gradient with a continuous interpolation. It is also represented in terms of bilinear basis functions.

$$l_{xx} = \sum_{j=1}^{m} L^j{}_{xx} \chi_j \; ; \; l_{xr} = \sum_{j=1}^{m} L^j{}_{xr} \chi_j \; ; \; l_{rr} = \sum_{j=1}^{m} L^j{}_{rr} \chi_j \; ; \; l_{rx} = \sum_{j=1}^{m} L^j{}_{rx} \chi_j \tag{23}$$

Once all the variables are represented in terms of the basis functions, the system of partial differential equations reduces to simultaneous algebraic equations for the coefficients of the basis functions of all fields. This set of equations is non-linear and sparse. It was solved by Newton's method, and quadratic convergence was obtained as the residual approached zero. The linear system of equations at each Newton iteration was solved using a frontal solver.

The domain was divided into 240 elements that correspond to 1035 nodes and 4860 degrees of freedom. A representative mesh is shown in Fig.(2), where is also shown the mapping between the physical and the reference frame.

4. Results

The amount of displaced liquid that remains on the capillary walls are usually reported in terms of mass fraction of liquid that is not displaced m, as defined in Eq. (1). The main goal of the present study is to analyze m and the the flow near the gas-liquid interface for some relevant dimensionless parameters as: Reynolds **N**umber $\mathrm{Re} \equiv \rho V_b D / \eta_c$; Capillary Number $Ca \equiv \eta_c V_b / \sigma$; Power-law index n and the Deborah Number $De \equiv \lambda V_b / R_o$.

In order to validate the theoretical model and the solution algorithm, the experimental results of Taylor (1960) for Newtonian liquid flowing slowly were recovered. This validation is shown in Fig. (4) that compares the fraction of mass deposited on the tube wall m predicted by the numerical simulation presented here with the measurements of Taylor (1960). The agreement is quite good over the entire range of capillary number.

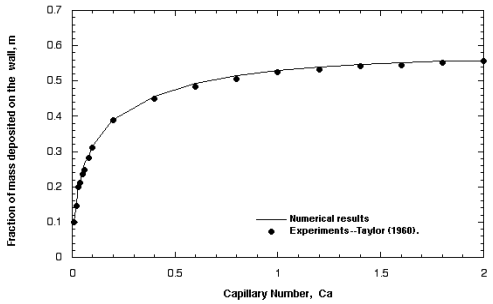

Figure 4. Fractional mass coverage as a function of capillary number for Newtonian Liquids with $\mathrm{Re} = 0$.

The streamlines of a Newtonian liquid at different capillary numbers are shown in Fig. (5). At high capillary number, the viscous force is stronger then the surface tension force and the adverse pressure gradient at the meniscus is small. There is no recirculation near the free surface and the film thickness left on the wall is relatively thick. As the capillary number decreases, the film thickness on the wall also decreases and a recirculation near the free surface appears. The three different patterns of streamlines suggested by Taylor (1960) do occur: One with no recirculation, at high capillary numbers; a second pattern with two stagnation points on the axis of the tube, obtained at moderate capillary numbers; and the third with a stagnation point at the tip of the bubble and a stagnation ring on the free surface.

The predicted interface configuration is also in good agreement with flow visualization reported by Cox (1964) and Huzyak and Koelling (1997), as illustrated in Fig. (6).

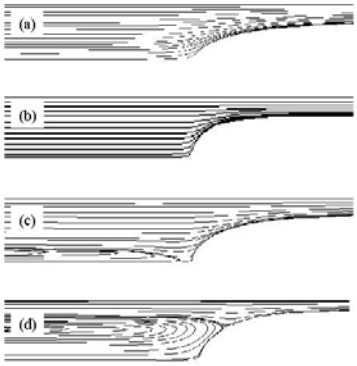

Figure 5. Streamline pattern near the free surface: (a) $Ca = 10$; (b) $Ca = 1$; (c) $Ca = 0.6$ and (d) $Ca = 0.2$

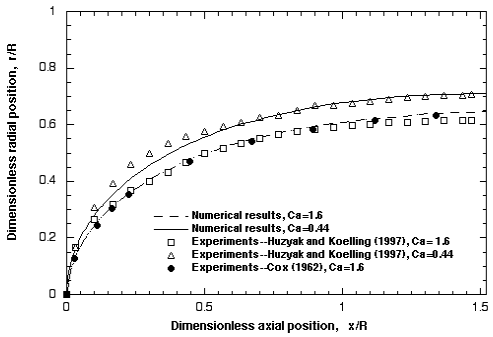

Figure 6. Comparison between predicted free surface profiles and experimental measurements.

The effect of Reynolds number for the gas-displacement of a Newtonian liquid is showed in Fig. (7). This figure shows the ratio between the liquid film deposited on tube wall relative to that predicted for slow displacement, $\mathrm{Re} = 0$. The simulations were done for a quite large range of Reynolds number, $0 \le \mathrm{Re} \le 450$, and for two values of capillary numbers, $Ca = 10$ and 0.6. Figure (7) shows that in very small Reynolds number, $\mathrm{Re} \le 1$ the gas-liquid displacement is dominated by the capillarity and no deviations from the case of $\mathrm{Re} = 0$ are observed. Furthermore, the maximum deviation is smaller than 20%, for high Reynolds numbers.

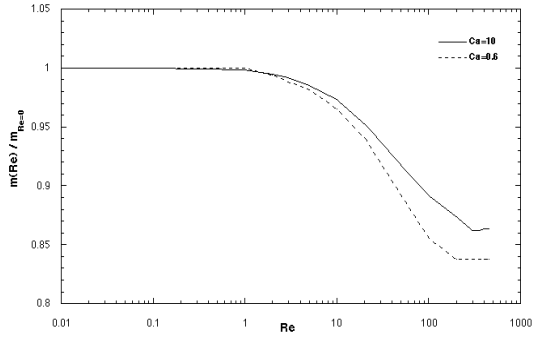

Figure 7. Fractional mass coverage as a function of Reynolds number for Newtonian Liquids with $Ca = 10$ and 0.6.

The effect of the Power Law index on the film thickness left on the wall is summarized in Fig. (8). It shows the predicted fractional mass coverage m as a function of capillary number obtained from gas penetration through a power-law liquid. The shear thinning behavior leads to thinner film deposited on the wall over the entire range of capillary number. This trend agrees qualitatively with the experimental data presented by Kamisli and Rayan (1999), however the measured thickness of the liquid film left on the wall is lower than the theoretical predictions. The perturbation method presented by Kamisli and Rayan (1999) could not correctly predict the variation of the residual liquid film as a function of the Power-Law index. A complete two-dimensional model of the flow, as the one presented

here is necessary to describe the non Newtonian flow near the free surface. One possible reason for the discrepancy between the theoretical results and the experiments is that viscosity dependence on shear rate of the two polymeric solutions used in the experiments, e.g. 1 % HEC and 1 % CMC, are not well described by a Power-Law function at the low deformation rate range. The Power-Law viscosity function can lead to unrealistic high viscosity at regions of the flow where the deformation rate is small.

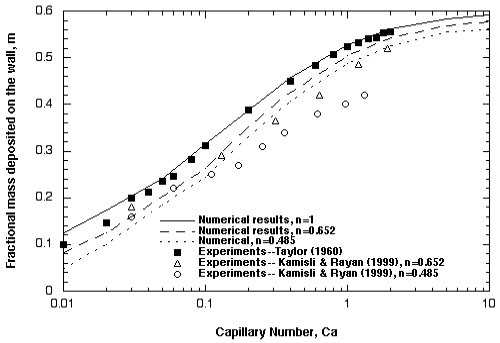

Figure 8. Fractional mass coverage as a function of capillary number for power-law liquids.

It is well known that the behavior of microstructured liquids in complex flows is very sensitive to the local kinematics. Polymer molecules behave quite differently in flow regions where the liquid is persistently stretched along the orientation of the molecules and in flow zones where the straining is oblique to molecular orientation. Thus, it is important to characterize the type of deformation suffered by liquid particles in different regions of the flow. The field of flow classification index R, defined in Eq. (13), for the gas displacement flow is shown in Fig. (9). Far from the gas liquid interface $R \approx 1$, indicating a shear dominated flow, as expected. The liquid layer left on the tube moves as a rigid body. i.e. plug flow, and the value of R is high in that region. Near the free surface, $R \approx 0$, indicating an extensional dominated flow.

According to Thompson et al. (2002), the extensional viscosity can be divided in two parts: one dissipative and other elastic as defined in Eq. (16). $\beta\eta_u$ represents the dissipative portion and $(1-\beta)\eta_u$ represents the elastic portion. Analyzing the fractional mass deposited on the tube wall, it was illustrated the qualitative difference between the dissipative and elastic effect of the extensional viscosity predicted by the algebraic model proposed by Thompson et al. (1999). The dissipative effect, $\beta = 1$, shown in Fig. (10), is obtained by vanishing α_3 and considering $\alpha_1 = 2\eta_s^R \eta_u^{1-R}$. The elastic effect, $\beta = 0$, is obtained by considering $\alpha_1 = 2\eta_s$ and vanishing ψ_1 and ψ_2. Thus, α_3 is calculated as $\alpha_3 = \left[4(T_R - 1)/\eta_s \dot{\varepsilon}\right](1-R)$.

The effect of the dissipative portion of the extensional viscosity on the ratio between the fractional mass deposited on the wall with a viscoelastic liquid to that of a Newtonian liquid as a function of the Deborah number is shown in Fig. (10). In that figure, the Deborah number is defined as $De = \lambda_u U / R$, where λ_u is a characteristic time as presented in Eq. (20). The Capillary number was fixed at $Ca = 10$. The change in the amount of liquid left on the wall is very small and the film thickness falls with Deborah number. This prediction does not agree with the experimental measurements of deposited film thickness with PEO solutions in water made by Huzyak and Koelling (1997). In their experiments, the fractional coverage m for the viscoelastic fluids begins to increase relative to the Newtonian results at $De \approx 1$, and it continues to rise with Deborah number for all $De > 1$. However, the predictions confirm the experimental results of Bonn and Meunier (1997). They compared the flow configuration and the film thickness left on the wall when gas is displacing two different polymeric solutions: PEO in water and Xanthan gum in water. The shear viscosity of the two solutions tested was matched by controlling the molecular weight and concentration of each solution. Both liquids presented non Newtonian extensional viscosity, with Trouton ratio larger than 3, however only the PEO solution showed an increase in the film thickness deposited on the wall when compared to the Newtonian case. The deposited film thickness of Xantham gum solution was very close to the one obtained when a Newtonian liquid is used. Because Xantham Gum is a rigid, rod-like polymer, the first normal stress coefficient is approximately zero. The theoretical predictions presented in Fig. (10) were obtained with $\psi_1 = \psi_2 = 0$ and therefore the model, considering only the dissipative portion of the extensional viscosity, is more suitable to describe rigid rod-like polymer solutions, such as Xantham gum.

The effect of the elastic portion of the extensional viscosity on the ratio between the fractional mass deposited on the wall with a viscoelastic liquid to that of a Newtonian liquid as a function of the Deborah number is presented in Fig. (11-a). The capillary number was fixed at $Ca = 10$. As before, the change in the amount of liquid left on the wall is very small, for the range of Deborah number analyzed. However, the film thickness arises with this parameter. This is

in agreement with the experimental results obtained by Huzyak and Koelling (1997) and Bonn and Meunier (1997) for PEO solutions. The convergence was obtained for a rather small range of Deborah number $0 \le De \le 0.02$. This limitation is very common in flow simulations of non Newtonian materials. Additionally, the presence of the free surface aggravates the problem of the convergence.

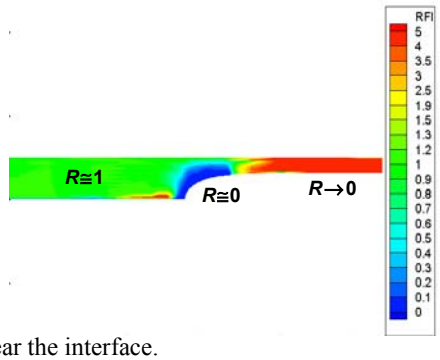

Figure 9. Flow classification index near the interface.

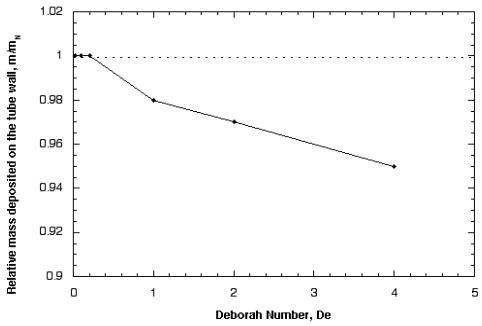

Figure 10. Fractional mass coverage as a function of Deborah number. Predictions obtained to analyze the dissipative effect of the viscoelastic viscosity.

Figure (11-b) shows the effect of the normal stress coefficients on the fractional mass deposited on the tube wall with respect to that of a Newtonian liquid. It is considered $\eta_u = \eta_s$ and $Ca = 10$. In this case, the characteristic time of the fluid is $\lambda_c = \psi_1 / 2\eta_0$. Again, the convergence was very difficult and, consequently, the range of Deborah number obtained was not sufficiently large, $0 \le De \le 0.4$. In any way, the predictions suggest a decrease on the film thickness left on the wall when the Deborah number increases.

The results presented on Fig. (11-a) and Fig. (11-b) indicate that the elastic portion of the extensional viscosity and the normal stress coefficient have an opposite effect on the fraction of mass deposited on the tube wall. It is clear that the range of Deborah number analyzed is, in fact, rather small and more simulations are necessary. However, a classical result presented by Debbaut and Crochet (1988) shows a similar relation between the effects of extensional viscosity and normal stress coefficients. They analyzed the flow of viscoelastic materials in abrupt contractions and found that the vortex length increases when the Trouton ratio is incremented while it decreases when the first normal stress difference rises.

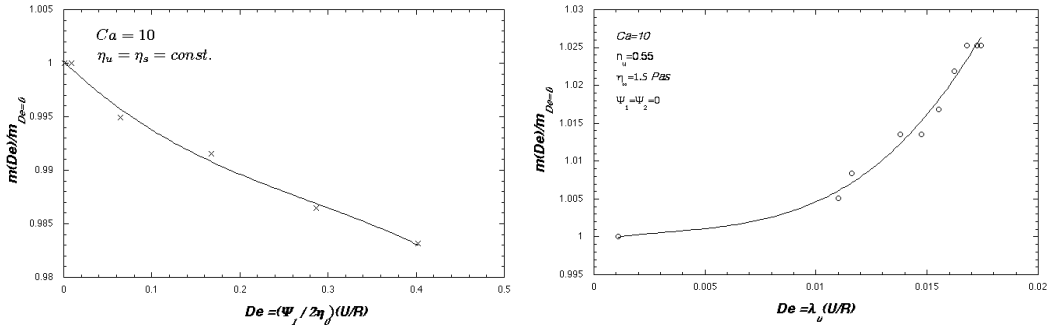

Figure 11. Fractional mass coverage as a function of Deborah number. a: Predictions obtained to analyze the normal stress coefficients. b: Predictions obtained to analyze the elastic effect of the extensional viscosity

5. Final Remarks

A two-dimensional model of the flow near the gas-liquid interface of a long bubble penetrating through a liquid in a capillary tube was presented. The presence of the free surface makes the solution of the problem complex; the domain where the differential equations are integrated is unknown *a priori*. A fully coupled formulation was used and the differential equations were solved by the Galerkin Finite Element Method.

Two different constitutive models were used: a simple Generalized Newtonian Liquid model with a power-law viscosity function and an algebraic model that takes into account the different behavior of polymer molecules in extension-dominated and shear dominated flow zones.

The thickness of the liquid film on the tube wall and the interface profile for Newtonian liquids in slow displacement, Re=0, agree with experimental data available in the literature. The effect of the Reynolds number was analyzed and it was observed that the liquid film deposited on the tube wall falls relatively to the case of slow motion for the same capillary number, when $\mathrm{Re} \geq 1$. However, the maximum deviation was smaller than 20%.

The predictions with the power-law model followed the same trends observed experimentally, which could not be predicted with a perturbation analysis. The qualitative difference between the theoretical and experimental results may be caused by the unrealistic high viscosity produced by the power-law equation in regions of the flow where the deformation rate is small.

The algebraic non Newtonian model was used to evaluate the effect of the dissipative and elastic portion of the extensional viscosity beyond the effect of the normal stress differences. The predictions show that the dissipative portion of the extensional viscosity and the normal stress differences have an opposite effect, on the fractional mass deposited on the tube wall, of that indicated by the elastic portion of extensional viscosity. In fact, the entire range of Deborah number analyzed is rather small and more accurate analysis is still necessary. However, results presented by Debbaut and Crochet (1988) also show an opposite effect of η_u and ψ_1.

The liquid film thickness left on the wall observed in experiments with Xanthan Gum solutions, which have a high Trouton ratio and vanishing normal stress difference, is very close to that of a Newtonian liquid as predicted by the hypothesis of the dissipative effect of the extensional viscosity.

Finally, the predictions suggest that the increment of the liquid film on the tube wall, relative to Newtonian case, is related to elastic effect of the extensional viscosity and not with normal stress differences, as generally presented.

6. Acknowledgment

This research was partially funded by grants from the Brazilian Science and Technology Secretary MCT, the Brazilian Research Council CNPq and by the State of Rio de Janeiro Research Foundation FAPERJ.

5. References

Astarita, G., 1979, J. Non-Newtonian Fluid Mechanics, vol. 6, pp.69-76.

Bretherton F. P., 1960, "The Motion of Long Bubble in Tubes", J. Fluid Mechanics, vol.10, pp.166-188.

Astarita, G., 1979, "Objective and Generally Applicable Criteria for Flow Classification", J. Non-Newtonian Fluid Mechanics, vol.6, pp. 69-76.

Cox, B. G., 1962, "On Driving a Viscous Fluid Out of a Tube ", J. Fluid Mechanics, pp.81-96.

Cox, B. G., 1964, "An Experimental Investigation of the Streamlines in Viscous Fluid Expelled from a Tube", J. Fluid Mechanics, vol.20, pp.193-200.

Debbaut B., Crochet M. J., 1988, "Extensional Effects in Complex Flows", J. Non-Newtonian Fluid Mechanics, vol.30, pp.169-184.

Fairbrother, F., Stubbs, A. E., 1935, J. Chem. Soc., vol.1, pp.527.

Gauri, V. , Koelling, K. W., 1999, "Gas-Assisted Displacement of Viscoelastic Fluids: Flow Dynamics at the Bubble Front", J. Non-Newtonian Fluid Mechanics, vol.83, pp.183-203.

Huzyak, P. C., Koelling, K. W., 1997, "The Penetration of a Long Bubble Through a Viscoelastic Fluid in a Tube", J. Non-Newtonian Fluid Mechanics, vol. 71, pp.73-88.

Kamisli, F., Ryan, M. E., 1999, "Perturbation Method in Gas-Assisted Power-Law Fluid Displacement in a Circular Tube and Retangular Channel", Chemical Engineering Journal, vol.75, pp.167-176.

Poslinski A. J., Coyle, D. J., 1994, "Steady Gas Penetration Through non Newtonian Liquids in Tube and Slit Geometries: Isothermal Shear Thinning Effects", Proc. Polymer Processing Society, 10 Annual Meeting, pp.219.

Taylor, G. I., 1960, "Deposition of a Viscous Fluid on the Wall a Tube", J. Fluid Mechanics, vol.10, pp.161-165.

Thompson, R. L., Souza Mendes, P. R., Naccache, M. F., 1999, "A New Constitutive Equation and its Performance in Contraction Flows", J. Non-Newtonian Fluid Mechanics, vol.86, pp.375-388.

Thompson, R. L., 2002, "Desempenho de uma nova equação constitutiva para líquidos não Newtonianos", Tese de Doutorado, Pontifícia Universidade Católica do Rio de Janeiro.

6. Copyright Notice

The author is the only responsible for the printed material included in his paper.